ACS APPLIED MATERIALS & INTERFACES

Research Article

www.acsami.org

# An Optical Sensing Strategy Leading to In Situ Monitoring of the Degradation of Mesoporous Magnetic Supraparticles in Cells

Dian Li,[†] Yuting Zhang,[†] Peng Yang,[†] Meng Yu,[†] Jia Guo,[†] Jennifer Q. Lu,[‡] and Changchun Wang*[,†]

[†]State Key Laboratory of Molecular Engineering of Polymers, Department of Macromolecular Science, and Laboratory of Advanced Materials, Fudan University, Shanghai, 200433, People's Republic of China

[‡]Materials Science and Engineering Department, School of Engineering, University of California at Merced, Merced, California 95343, United States

**ABSTRACT:** Mesoporous magnetic supraparticles (meso-MSPs) as multifunctional targeted drug carriers have attracted much attention, because of their easy magnetic-field manipulation and in situ sensing functionality. In this paper, a $Fe^{3+}$-selective chemodosimeter fluorescent probe (FP-1) was synthesized and loaded inside of the meso-MSPs (meso-MSPs/probe); the meso-MSPs/probe nanocomposites were then used to monitor the degradation of meso-MSPs in cells. In our experiments, strong fluorescence intensity was observed in HeLa cells, because of their acidic intracellular environment, which can quickly degrade the meso-MSPs and then release $Fe^{3+}$ ions in cells that, in turn, activate the fluorescence of FP-1. Meanwhile, a very weak fluorescence signal was detected in HEK 293T cells due to the relative neutral intracellular environment of HEK 293T cells, which prevented the $Fe^{3+}$ ion from leaching out of meso-MSPs. Moreover, this degradation−luminescence relationship of the meso-MSPs/probe nanocomposites not only assisted us to understand the degradation status of meso-MSPs in cells, but also allowed us to recognize the peculiarity of different cells with various intracellular environments.

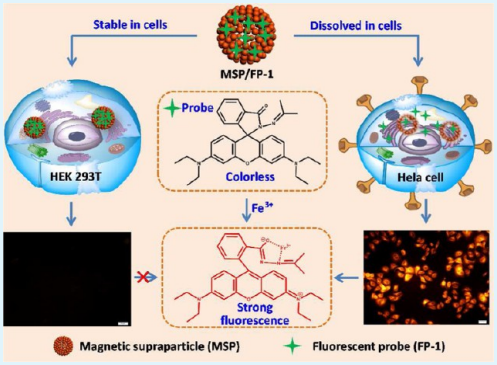


**KEYWORDS:** *magnetic supraparticles (MSPs), $Fe^{3+}$-sensitive fluorescent probe, bio-degradation, in situ monitoring, drug carrier*

## 1. INTRODUCTION

Magnetic functional nanoparticles as site-specific drug carriers have attracted much attention during the past decades,[1−4] since they can be easily manipulated by external magnetic fields and targeted to special tissues.[5,6] In addition, based on the different conditions between intracellular and extracellular environment, the environmental-response functional layer integrated in drug carriers have been extensively investigated, including pH-sensitive,[7,8] redox-sensitive,[9] and temperature-sensitive[10] materials. To endow the nano-carriers with more useful functionalities, magnetic nanoparticles are usually integrated with smart functional shells, such as silica,[11,12] metal oxides[13,14] and environmental-sensitive polymers,[15,16] for constructing multifunctional drug carriers with well-defined structures. With the smart shell composited in, the magnetic nano-carriers can be endowed with high drug loading capacity, controlled drug release, and good targeting ability.[17,18] However, the cumbersome synthetic steps and low saturation magnetization are obstacles for their practical applications. Besides, the demand of the biodegradability for the composite nano-carriers is another challenge for their practical use.[19−21]

Recently, one-step solvothermal methods have been employed to prepare the mesoporous magnetic supraparticles (meso-MSPs) that possess good colloidal stability and biodegradability by using natural polymer as the stabilizers, such as poly(amino acid)[22] and glycan.[23] The meso-MSPs not only possess excellent dispersion stability in aqueous solutions,[24,25] but also create other novel properties, such as mesoporosity and acid degradability. The high surface area of the meso-MSPs affords an ideal depository for hosting guest molecules. The acid-degradable materials will eliminate the accumulation problem in the body following the drug delivery. Although the simulated cellular experiments have proven its degradability,[22,23] the direct and visualized experimental results have never been reported for in situ monitoring of the degradation of meso-MSPs in cells until now.

Luminescence-based bio-imaging is considered as a convenient approach for visualizing the morphological details of tissues and the intracellular structures.[26−28] In recent years, fluorescent chemodosimeters in bio-imaging have attracted increasing attention and become a very active research field, because of their rapid response, high sensitivity, and excellent selectivity.[29−31] As a powerful tool, chemodosimeters have been widely used to detect analytes through an irreversible chemical reaction between the sensitizer molecule and the analytes, especially for the detection of heavy metals, which will damage organisms if they accumulate in the body. Fluorescent chemodosimeters selectively responding to specific metal ions, such as $Hg^{2+}$,[32] $Cu^{2+}$,[33] $Fe^{3+}$,[34] $Cr^{3+}$,[35] $Pb^{2+}$,[36] $Fe^{2+}$,[37] and $Zn^{2+}$,[38] have been widely reported. Because of the

Received: July 10, 2013
Accepted: November 25, 2013
Published: November 25, 2013

  

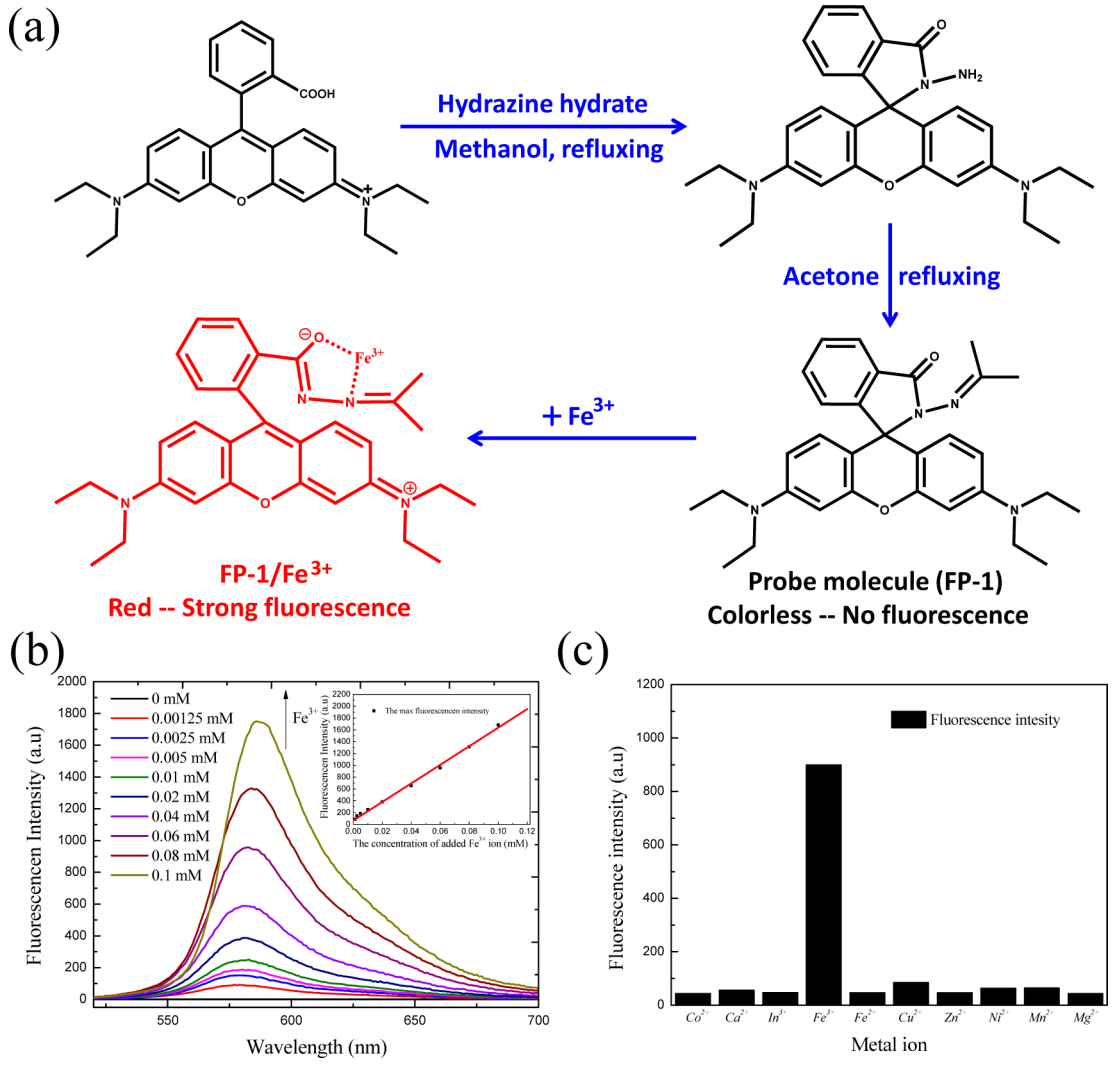


**Figure 1.** (a) Synthetic scheme for fluorescent probe (FP-1) and the schematic representation of the $Fe^{3+}$-induced ring-opening structure of rhodamine-based probe (FP-1/$Fe^{3+}$). (b) Fluorescence spectra of 0.25 mM rhodamine-based fluorescent probe (FP-1) in aqueous solution with various $Fe^{3+}$ ion concentrations. (Insert shows the corresponding plot of fluorescent emission intensity at 582 nm as a function of $Fe^{3+}$ ion concentration.) (c) The fluorescence intensity of 0.25 mM rhodamine-based fluorescent probe (FP-1) in various 0.04 mM metal ion solution. All the excitation wavelengths were 510 nm.

importance of $Fe^{3+}$ in organisms, an increasing number of research on fluorescent chemodosimeters for $Fe^{3+}$ are being reported, whose fluorescence mechanism can be classified into three types: (1) $Fe^{3+}$-induced spirolactam ring-opening process;[39] (2) $Fe^{3+}$-induced spirolactam ring-opening and hydrolysis processes;[40] and (3) $Fe^{3+}$-induced oxidation and hydrolysis reaction processes.[41] Moreover, some $Fe^{3+}$-selective chemodosimeters have already been successfully applied for monitoring the existence of $Fe^{3+}$ ions in living cells.[39,40,42]

Herein, by harnessing the synergistic effect of the rhodamine-based $Fe^{3+}$ fluorescent sensor and the degradation of meso-MSPs, we successfully designed a new type of composite nanoparticles (meso-MSPs/probe) to monitor the degradation process of meso-MSPs in living cells for the first time. Moreover, these $Fe^{3+}$-sensitive composite nanoparticles also could be used to monitor the various pH environments in different cells based on the fluorescent state.

## 2. EXPERIMENTAL SECTION

**2.1. Materials.** Iron(III) chloride hexahydrate ($FeCl_3 \cdot 6H_2O$), ammonium acetate ($NH_4OAc$), ethylene glycol (EG), anhydrous ethanol, anhydrous methanol, and anhydrous acetone were purchased from Shanghai Chemical Reagents Company and used as received. Poly($\gamma$-glutamic acid) (PGA) was purchased from Dingshunyin Biotechnology Company (China) and used as received. Hydrazine ($NH_2NH_2 \cdot H_2O$) was purchased from Sinopharm Chemical Reagent Corp. Rhodamine B was purchased from Aladdin (Shanghai, China). Dulbecco's modified Eagle's medium (DMEM), fetal bovine serum (FBS), penicillin G, streptomycin, and trypsinase were obtained from GIBCO BRL (Grand Island, NY). Deionized water was used in all experiments. All other chemicals were available commercially and used without further purifications.

**2.2. Synthesis of $Fe^{3+}$-Selective Sensitive Rhodamine-Type Fluorescence Probe.** The $Fe^{3+}$-sensitive rhodamine-type fluorescence probe (FP-1) was synthesized according to the published procedure, as shown in Figure 1a.[39,42] Firstly, 0.8 g of rhodamine B was dissolved in 30 mL of methanol, and an

excess of hydrazine hydrate (1.0 mL) was added. The reaction solution then was refluxed at 70 °C until the transparent solution changed from pink to orange. After cooling to room temperature, the reaction liquid was poured into 30 mL of water, and it was then extracted with 25 mL of ethyl acetate. This process was repeated five more times. The extracts were dried with anhydrous sodium sulfate, filtered, and then evaporated. The product was washed with water and air-dried to give an orange powder. Secondly, all the orange powder was dissolved in 50 mL of acetone, followed by refluxing for 2 h. After all the acetone was evaporated under reduced pressure, the crude powder was dried and purified by column chromatography ($CH_2Cl_2$:$CH_3OH$ = 5:1, v/v) to get the colorless $Fe^{3+}$-selective sensitive rhodamine-type fluorescein probe. $^1H$ NMR ($\delta$, $CDCl_3$, ppm): 7.89−7.92 (m, 1H), 7.42−7.47 (m, 2H), 7.09−7.13 (m, 1H), 6.53 (d, $J$ = 8.8 Hz, 2H), 6.38 (d, $J$ = 2.4 Hz, 2H), 6.26−6.29 (dd, $J$ = 8.8 Hz , $J$ = 2.8 Hz, 2H), 3.30−3.35 (m, 8H), 1.96 (s, 3H), 1.81 (s, 3H), 1.16 (t, 7.2 Hz, 12H).

**2.3. Preparation of Mesoporous Magnetic Supraparticles (Meso-MSPs).** The mesoporous magnetic supraparticles (meso-MSPs) were prepared by the solvothermal method.[22] 1.35 g (5 mmol) of $FeCl_3{\cdot}6H_2O$ and 0.80 g of PGA were dissolved in 70 mL of ethylene glycol. After 3.85 g (0.05 mol) of $NH_4OAc$ was added, the mixture was stirred vigorously for 1 h at 160 °C to form a homogeneous brownish solution and then transferred into a Teflon-lined stainless-steel autoclave (100 mL capacity). The autoclave was heated to 200 °C and maintained for 16 h. After it was cooled to room temperature, the black MSPs were then rinsed five times with ethanol under ultrasonic conditions to effectively remove the reagents that did not react. The meso-MSPs were separated from the supernatant by using magnetic force during each rinsing step.

**2.4. Preparation of Meso-MSPs/Probe and HMS/Probe.** Twenty-five milligrams (25 mg) of meso-MSPs were ultrasonically dispersed in 10 mL of a probe methanol solution (2 mg/mL), followed by mechanical stirring for 4 h. After that, 10 mL of water was added drop by drop and then the solution was stirred for an additional 24 h, which enabled the gradual migration of the probe into the pores of meso-MSPs. The resultant particles were separated by a magnet and were washed with a PBS buffer (pH 7.4) until the supernatant was colorless with $Fe^{3+}$ solution dropping in, and then this product was freeze-dried for 3 days. The hollow mesoporous silica (HMS)/probe was prepared by the same procedure described above, where the HMS was synthesized following the procedure of the Yang group,[43] while the meso-MSPs were replaced by HMS and the separation method was altered to centrifugation.

**2.5. Acid-Degradable Experiment of Meso-MSPs/Probe.** Five milligrams (5 mg) of meso-MSPs/probe nanospheres were dispersed in 50 mL of 0.1 M $Na_3Cit/H_3Cit$ buffer (pH 5.0 or pH 7.4), and then shaken in a table concentrator at 200 rpm. After predetermined intervals, 3 mL of solution was taken out. The undegraded MSPs were separated with the assistance of an external magnetic field. The concentration of $Fe^{3+}$ ion in every supernatant was determined by inductively coupled plasma (ICP) spectroscopy and the fluorescence property of each supernatant was measured by fluorescence spectroscopy.

**2.6. In Vitro Cytotoxicity Experiment.** In vitro cytotoxicity of meso-MSPs and meso-MSPs/probe were assessed on HEK 293T cells and HeLa cells, using the CCK8 method. Specifically, 100 $\mu$L of cells were seeded on a 96-well flat culture plate at a density of $1 \times 10^4$ cells per well and subsequently incubated for 24 h to allow attachment. Then samples with different concentrations (1.0, 5.0, 10, 50, 100 $\mu$g/mL) were added to each group (three wells) for 24 h. After removing the previous nutrient solution, the cells were incubated in 110 $\mu$L of DMEM containing 10 $\mu$L CCK-8 solution for 1 h. The absorbance of the suspension was measured at 450 nm on an ELISA reader. Cell viability was calculated by means of the following formula:

$$\text{cell viability}\,(\%) = \frac{OD_{450(\text{sample})} - OD_{450(\text{blank})}}{OD_{450(\text{control})} - OD_{450(\text{blank})}} \times 100$$

**2.7. Cell Staining Experiment.** The cell staining experiment by probe FP-1 was measured by fluorescence microscope. The HeLa cells first were incubated in a cell culture chamber with DMEM containing $FeCl_3$ (0.01 mM) for 2 h, then the cells were washed with DMEM and PBS to remove the $FeCl_3$ that did not enter the cells prior to fluorescence observation. After that, the $Fe^{3+}$-containing HeLa cells were incubated with FP-1 probe (0.02 mM) for 0.5 h, followed by washing with DMEM and PBS to remove the probes that did not enter the cells. Meanwhile, a parallel test was done using the same method, but with alteration of the addition order of $FeCl_3$ and FP-1 probe. All fluorescence images were taken with an excitation wavelength of 520 nm and an exposure time of 10 ms.

The behaviors of cells treated with meso-MSPs/probe, HMS/probe, meso-MSPs were also measured by fluorescence microscopy. The HeLa cells and HEK 293T cells were incubated in a cell culture chamber with the meso-MSPs/probe (0.05 mg/mL), HMS/probe (0.05 mg/mL), meso-MSPs (0.05 mg/mL). For meso-MSPs/probe and HMS/probe, the cells were washed with DMEM and PBS to remove the free nanoparticles and free probes that did not enter the cells prior to fluorescence observation at predetermined intervals. For meso-MSPs, the cells were washed with DMEM and PBS to remove the free nanoparticles that did not enter the cells at any given predetermined intervals, followed by incubating in 0.5 mL of DMEM-containing probes (0.015 mg) for staining prior to fluorescence observation.

The fluorescence intensity of HeLa cells and HEK 293T cells was measured by flow cytometer analysis. The HeLa cells and HEK 293T cells were incubated in a cell culture chamber with the meso-MSPs/probe (0.05 mg/mL). After incubation, the cells were washed with PBS to remove the free nanoparticles or free probes that did not enter the cells, and then were taken out by the digestion of pancreatic enzyme, followed by washing with PBS to remove the DMEM and pancreatic enzyme. Finally, the cells were dispersed with 0.25 mL PBS in a flow cell tube for the flow cytometer experiment. The excitation wavelength was 488 nm and the emission wavelength was 580 nm.

**2.8. Characterization.** The fluorescence images were obtained on a Model IX71 fluorescence microscope (Olympus, Tokyo, Japan) and a Model FV1000 confocal laser scanning microscope (Olympus, Tokyo, Japan). High-resolution transmission electron microscopy (HRTEM) images were taken on a Model JEM-2010 transmission electron microscope (JEOL, Japan) at an accelerating voltage of 200 kV. Samples dispersed at an appropriate concentration were cast onto a carbon-coated copper grid. Scanning electron microscopy (SEM) measurements were performed using a Model TS-5136MM scanning

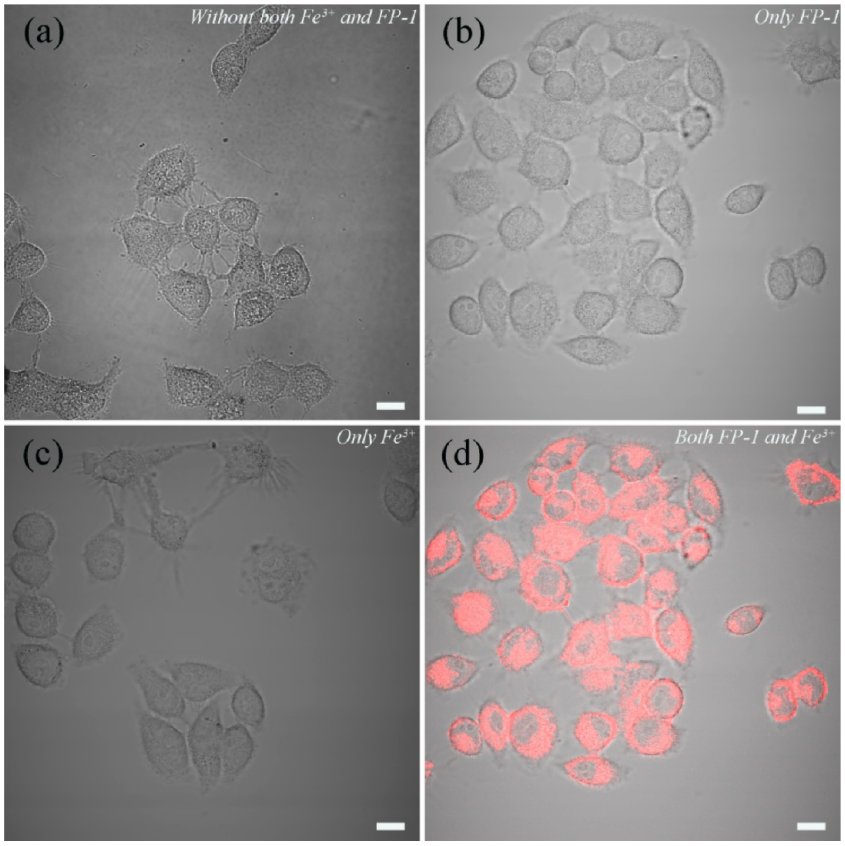


**Figure 2.** Merged bright-field and fluorescence field images of confocal laser scanning microscopy (CLSM): (a) HeLa cell, (b) HeLa cells incubated with only FP-1, (c) HeLa cells incubated with only $Fe^{3+}$, and (d) HeLa cells incubated with both $Fe^{3+}$ and FP-1. The excitation wavelength was 546 nm; all the scale bars are 5 $\mu$m.

electron microscope (TESCAN, Czech Republic) at an accelerating voltage of 20 kV. Samples dispersed at an appropriate concentration were cast onto a glass sheet at room temperature and sputter-coated with gold. Magnetic characterization was carried out on a Model 6000 physical property measurement system (Quantum Design, San Diego, CA, USA) at 300 K. Fourier transform infrared (FT-IR) spectra were recorded on a Model Magna-550 spectrometer (Nicolet, USA), where the samples were dried and mixed with KBr to be compressed to a plate for measurement. Thermogravimetric analysis (TGA) data were obtained on a Model Pyris-1 thermal analysis system (Perkin–Elmer, Eden Prairie, MN, USA) under a flowing nitrogen atmosphere and at a heating rate of 20 °C/min from 100 °C to 800 °C. $^1$H NMR spectrum was obtained on a Mercury Plus 400 MHz spectrometer with $CDCl_3$ as the solvent and tetramethylsilane (TMS) as the internal standard. The fluorescence emission spectra were recorded with a Model RF-5301PC spectrometer under the excitation wavelength of 365 nm (Shimadzu, Japan). Inductively coupled plasma–atomic emission spectrometry (ICP-AES) was performed on a Model P-4010 spectrometer (Hitachi, Japan). Flow cytometer analysis was performed on a FACSAria II (Becton–Dickinson, San Jose, CA, USA), with an excitation wavelength of 488 nm and the emission wavelength of 580 nm.

## 3. RESULTS AND DISCUSSION

**3.1. Synthesis and Properties of $Fe^{3+}$-Sensitive Rhodamine-Based Fluorescence Probe (FP-1).** The $Fe^{3+}$-sensitive rhodamine-based fluorescent probe (FP-1) was synthesized as shown in Figure 1a. The as-prepared probe FP-1 with a closed-whorls structure does not fluoresce, because of the blocking of the extended $\pi$-conjugation of rhodamine.[28,39] However, once the probe FP-1 encounters $Fe^{3+}$ ion, a strong fluorescence signal can be detected. Moreover, the fluorescence intensity enhanced with the increase of $Fe^{3+}$ ion concentration (Figure 1b), i.e., the fluorescence intensity of the probe FP-1 was linearly dependent on the concentration of the $Fe^{3+}$ ion (see the inset of Figure 1b), which is attributed to the delocalized xanthene moiety of the ring-open amide form of FP-1 that recovered the extended $\pi$-conjugation of rhodamine (Figure 1a). But when the $Fe^{3+}$ ion was replaced with other metal ions, such as $Cu^{2+}$, $Co^{2+}$, $Ni^{2+}$, $In^{3+}$, $Zn^{2+}$, $Ca^{2+}$, $Mg^{2+}$, $Mn^{2+}$ or $Fe^{2+}$, the FP-1 was still in quenching state with very low fluorescence, which demonstrated that the FP-1 was selective and sensitive to $Fe^{3+}$ (Figure 1c). To investigate the imaging capability of the synthesized FP-1, HeLa cells were incubated with $Fe^{3+}$ ions and probe FP-1. The experimental results showed that the fluorescence signal could only be detected when HeLa cells were incubated with both $Fe^{3+}$ ion and probe FP-1 (Figure 2d). No fluorescence was observed in the absence of either $Fe^{3+}$ ion or probe FP-1 (Figures 2a–c), illustrating that the generation of fluorescence cannot be short of either $Fe^{3+}$ ions or FP-1.

**3.2. Preparation of Degradable Mesoporous Magnetic Supraparticles (Meso-MSPs).** Mesoporous magnetic supraparticles (meso-MSPs) were prepared by a one-step solvothermal method.[22] From the transmission electron microscopy (TEM) and scanning electron microscopy (SEM) images, we can find that the poly($\gamma$-glutamic acid) (PGA)-stabilized meso-MSPs possess uniform shape and a rough

surface, and have an average size of ~120 nm (see Figures 3a and 3b). Nitrogen adsorption−desorption isotherms of meso-

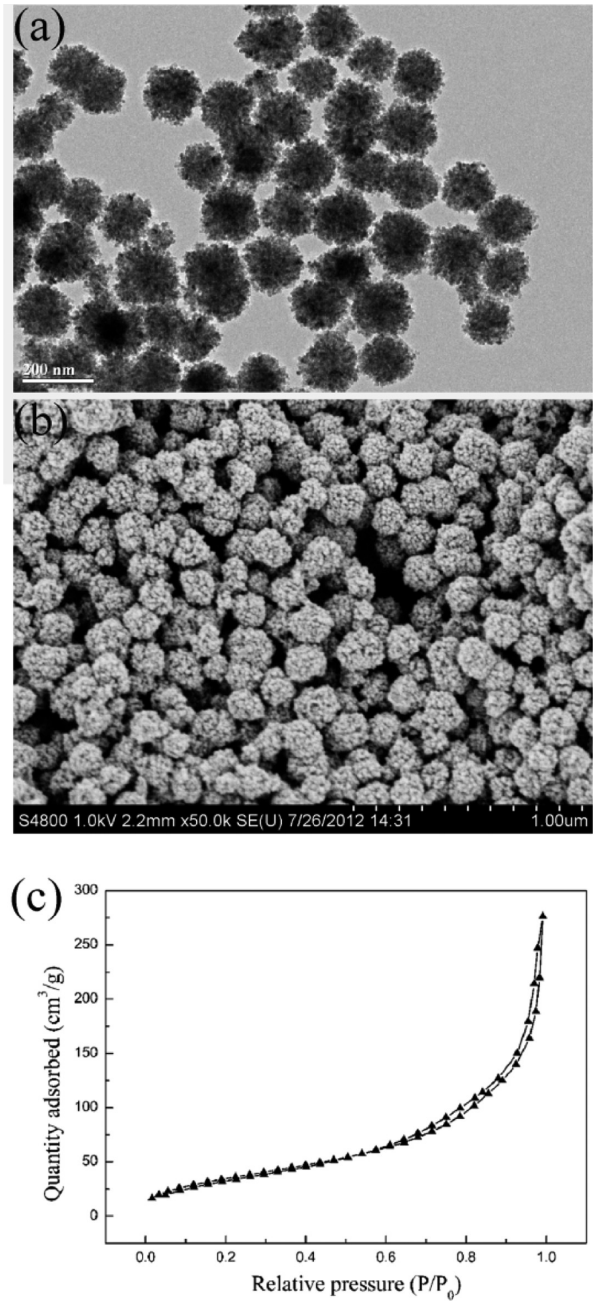


**Figure 3.** (a) Transmission electron microscopy (TEM) and (b) scanning electron microscopy (SEM) images of meso-MSPs. (c) Nitrogen adsorption−desorption isotherms of meso-MSPs.

MSPs revealed that they have a mesoporous structure (Figure 3c). The Brunauer−Emmett−Teller (BET) surface area and total pore volume were calculated to be 147.7 $m^2/g$ and 0.427 $cm^3/g$, respectively, demonstrating that the meso-MSPs can provide sufficient space for guest molecules storage and delivery.

**3.3. Loading of Fluorescent Probe (FP-1) in Mesoporous MSPs (Meso-MSPs/Probe).** In order to examine their behavior in cells, the fluorescent probe (FP-1) was loaded in meso-MSPs by the nanoprecipitation method. Experimental evidence for the loading was provided by Fourier transform infrared spectroscopy (FT-IR) and vibrating sample magnetometry (VSM) in Figures 4a and 4b. After FP-1 was loaded, both

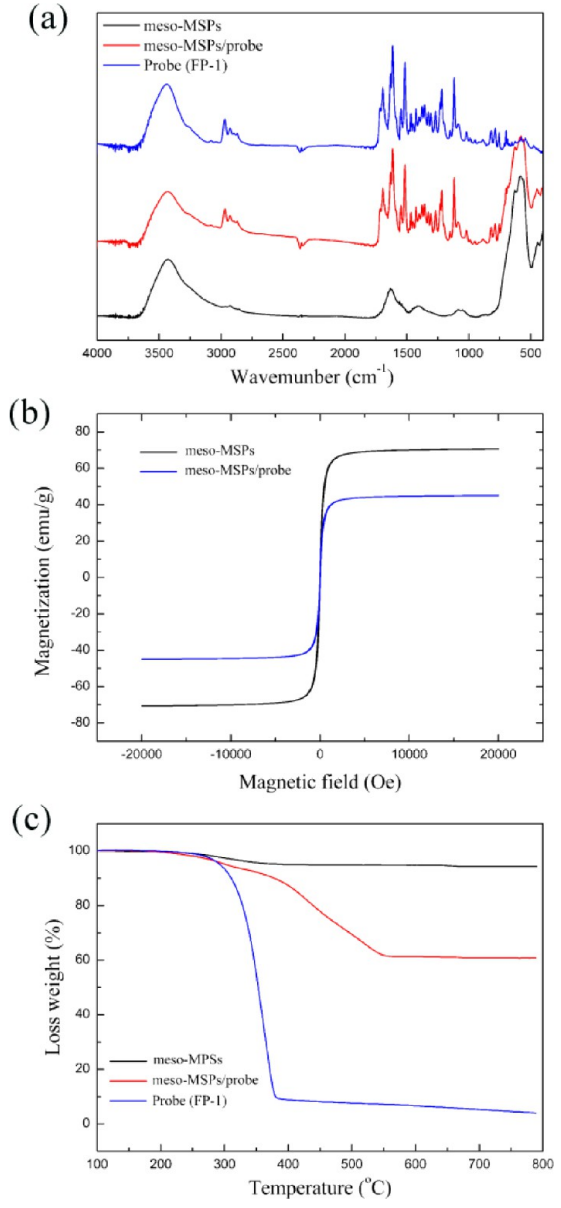


**Figure 4.** (a) Fourier transform infrared spectroscopy (FT-IR) spectra of meso-MSPs, meso-MSPs/probe, and probe FP-1. (b) Vibrating sample magnetometry (VSM) curves of meso-MSPs and meso-MSPs/probe. (c) Thermogravimetic analysis (TGA) analysis of meso-MSPs, probes, and meso-MSPs/probe in $N_2$.

characteristic peaks of the FP-1 and meso-MSPs could be clearly observed in the FT-IR spectra of the meso-MSPs/probe. The peak at 586 $cm^{-1}$ corresponded to the stretching vibration modes of Fe═O in $Fe_3O_4$, and the cuspidal peaks from 1000 $cm^{-1}$ to 1800 $cm^{-1}$ corresponded to the complex structure of FP-1. Meanwhile, the saturation magnetization value decreased from 71.5 emu/g to 43.1 emu/g, and the superparamagnetism of the nanocomposite was still retained. Moreover, the loading amount of FP-1 calculated from thermogravimetric analysis (TGA) was ~30%, and the hysteretic weight loss of FP-1 in meso-MSPs/probe suggested that the probes were filled in the mesoporous channels (Figure 4c).


dx.doi.org/10.1021/am4043596 | ACS Appl. Mater. Interfaces 2013, 5, 12329−12339

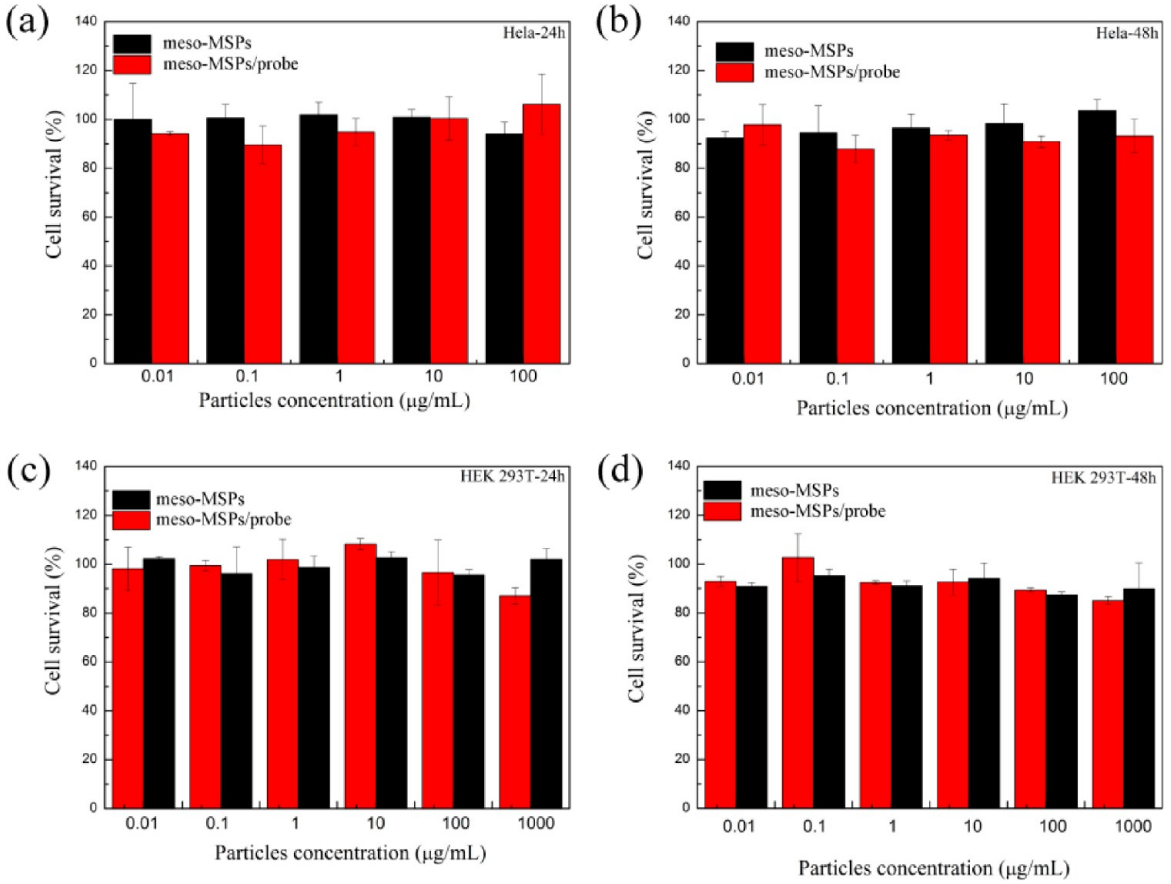


**Figure 5.** Cell survival of (a, b) HeLa cells and (c, d) HEK 293T cells after incubation with different concentrations of meso-MSPs and meso-MSPs/probe for 24 h and 48 h, respectively.

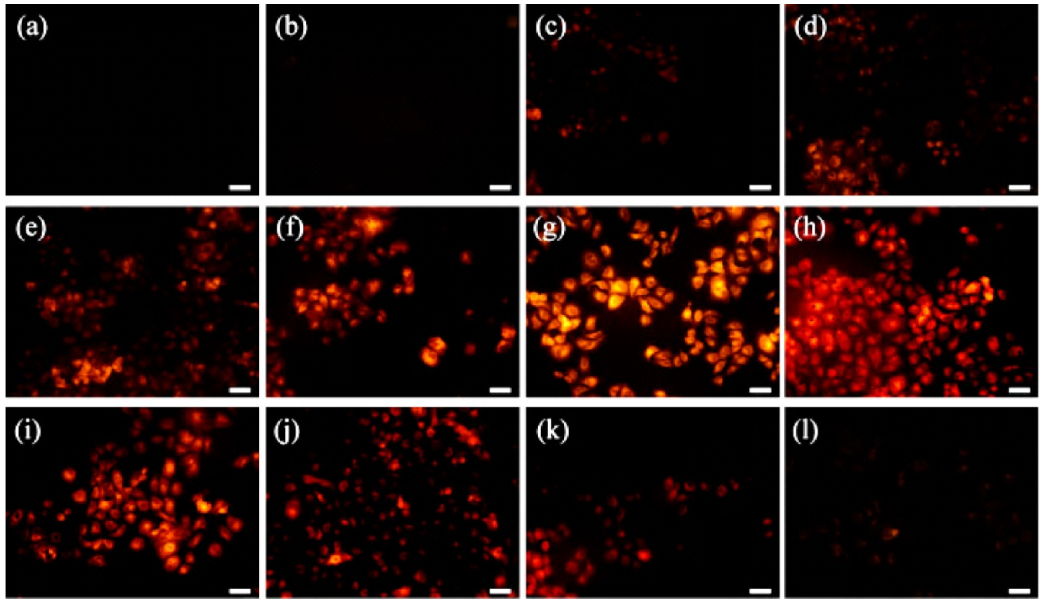


**Figure 6.** Fluorescence microscope images of HeLa cells incubated with meso-MSPs/probe for (a) 0, (b) 2, (c) 5, (d) 18, (e) 24, (f) 48, (g) 72, (h) 96, (i) 120, (j) 144, (k) 192, and (l) 240 h. The excitation wavelength was 520 nm; all the scale bars are 20 $\mu$m, and the exposure time was 10 ms.

**3.4. Degradable Behaviors of Meso-MSPs/Probe in HeLa Cells Monitored by $Fe^{3+}$-Sensitive Probe (FP-1).** Our earlier work demonstrated that the meso-MSPs are acid-degradable.[22] Since the direct evaluation of their degradability is critical to drug delivery, we thus chose HeLa cells and HEK 293T cells to investigate the degradation of meso-MSPs, using FP-1 as a fluorescent probe. The in vitro cytotoxicity showed that both the meso-MSPs and meso-MSPs/probe were nontoxic (Figure 5). When the meso-MSPs/probe was incubated with HeLa cells, no fluorescence signal could be

detected at the beginning (Figure 6a). When the incubation time reached 2 h, very weak fluorescence was detected (Figure 6b), which became much more intense when the incubation time was extended to 5 h (Figure 6c). As the incubation time was prolonged, the intensity of fluorescence became stronger and stronger (see Figures 6d–h). On the other hand, after 4 days of incubation, the trend of fluorescence intensity in HeLa cells started to decrease gradually (see Figures 6i–6k), with almost no fluorescence observable after 10 days (see Figure 6l). The fluorescence in the cells indicated that the probe FP-1 had attached to the $Fe^{3+}$ ion, which was released from the meso-MSPs. This result suggested that the simultaneous release both of probe FP-1 and the $Fe^{3+}$ ion from meso-MSPs in Hela cells, and the increase of fluorescence intensity with time further proved the gradual dissolution of meso-MSPs within the intracellular environment of HeLa cells. The weakening of the fluorescence intensity after four days of incubation might suggest the probe/$Fe^{3+}$ ion has been metabolized or the excessive $Fe^{3+}$ may result in fluorescence quenching, which will be explained in the last part of this paper.

In order to further prove the function of the $Fe^{3+}$ ion, we replaced the meso-MSPs with hollow mesoporous silica (no Fe atom) as the carrier of probe FP-1 (HMS/probe).[43] When the HeLa cells were incubated with HMS/probe, no fluorescence signal could be detected throughout the entire incubation time (see Figures 7a and 7b). However, if the HeLa cells were

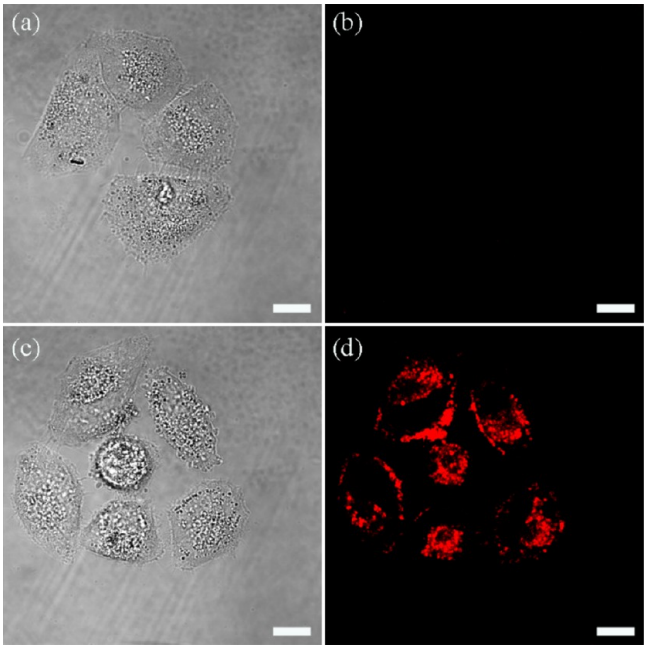


**Figure 7.** Confocal laser scanning microscope (CLSM) images of HeLa cells (a, b) incubated with HMS/probe for 24 h and (c, d) then treated with 0.01 mM $FeCl_3$/PBS for 1 h, followed by removal of the HMS/probe not entering cells. The excitation wavelength was 546 nm; all the scale bars are 5 $\mu$m.

treated with 0.01 mM $FeCl_3$/PBS for 1 h, red fluorescence was presented clearly in cytoplasm (Figures 7c and 7d); this result hinted that the probe was discharged from the carrier to the cells, so the absence of fluorescence could be ascribed to the lack of $Fe^{3+}$ ions, implying that the dissolution of $Fe^{3+}$ ions from meso-MSPs is one of the key parameters for the fluorescence. In addition, when HeLa cells were incubated with meso-MSPs alone, the fluorescence signal was not detectable (Figure 8, control); however, if the above HeLa cells were further treated with FP-1 molecules for 30 min, the fluorescence in cells appeared again (see Figures 8a–g). With extended incubation time, the fluorescence intensity increased at first and then declined, which was the same as the result observed for meso-MSPs/probe in cells, as shown in Figure 2. It is also worth pointing out that the fluorescence intensity of this extrinsic staining method was weaker than that using meso-MSPs/probe at the same probe concentration. Since the probe is hydrophobic, it cannot be readily incorporated into the cells by itself, which also suggested that the meso-MSPs can effectively enhance the deliverability of guest molecules to cells.

**3.5. Degradable Behaviors of Meso-MSPs/Probe in HEK 293T Cells Compared with HeLa Cells.** To compare the intracellular environment of cancer cells (HeLa cells) with normal cells (HEK 293T cells), we further investigated the behavior of meso-MSPs/probe in HEK 293T cells. When HEK 293T cells were incubated with meso-MSPs/probe, no clear fluorescence signal could be detected throughout the entire incubation period. Regardless of whether the incubation time was 24 h or 72 h, only very faint fluorescence signals could be detected in some of the cells (Figures 9g–i). In contrast, the fluorescence signal of meso-MSPs/probe in HeLa cells was much stronger in the same incubation time (Figures 9a–c).

In addition, flow cytometry (FCM) was employed to quantitatively track the fluorescence intensity of these two types of cells (see Figures 9d–f and Figures 9j–l). With prolonged incubation time, the fluorescence intensity of HeLa cells increased progressively, while the fluorescence intensity of HEK 293T cells remained approximately the same, corroborating the results of fluorescence microscope images. The stark contrast of the degradation behavior between these two types of cells can be attributed to the different intracellular pH values.[44,45] According to the previous report, meso-MSPs would degrade completely in a pH 5.0 buffer but disperse stably in a pH 7.4 buffer;[22] these pH values are close to the HeLa and HEK 293T intracellular environments, respectively. Generally, the meso-MSPs/probe will be introduced to cells through endocytosis, and subsequently the fluorescent probes are released from meso-MSPs to cells gradually. As for the HeLa cells, the meso-MSPs could be dissolved in the relatively lower pH intracellular environment[44,45] and then $Fe^{3+}$ ions would be produced. The interaction of the fluorescent probe with $Fe^{3+}$ ions in HeLa cells produced the fluorescence, which could increase as more and more $Fe^{3+}$ ions were dissolved from the meso-MSPs with prolonging the incubation time in HeLa cells. However, for the HEK 293T cells, meso-MSPs could not be obviously degraded under the relative neutral intracellular environment in a short time, and only a very small amount of $Fe^{3+}$ ions could be released. Thus, the probe could not emit fluorescence to light the HEK 293T cells, because of the lack of $Fe^{3+}$ ions. The detailed description for this process has been depicted in Scheme 1.

**3.6. Degradable Behaviors of Meso-MSPs/Probe in a Simulated Cellular Environment.** In order to verify our conjecture that intracellular pH is responsible for the differences in fluorescence behaviors, two different buffer solutions—pH 7.4 and pH 5.0—were used to emulate the intracellular environments of these two types of cells. Figure 10a contains a set of the fluorescence spectra as a function of time. We found that there was no detectable fluorescence signal in the pH 7.4 buffer solution, while gradually enhanced

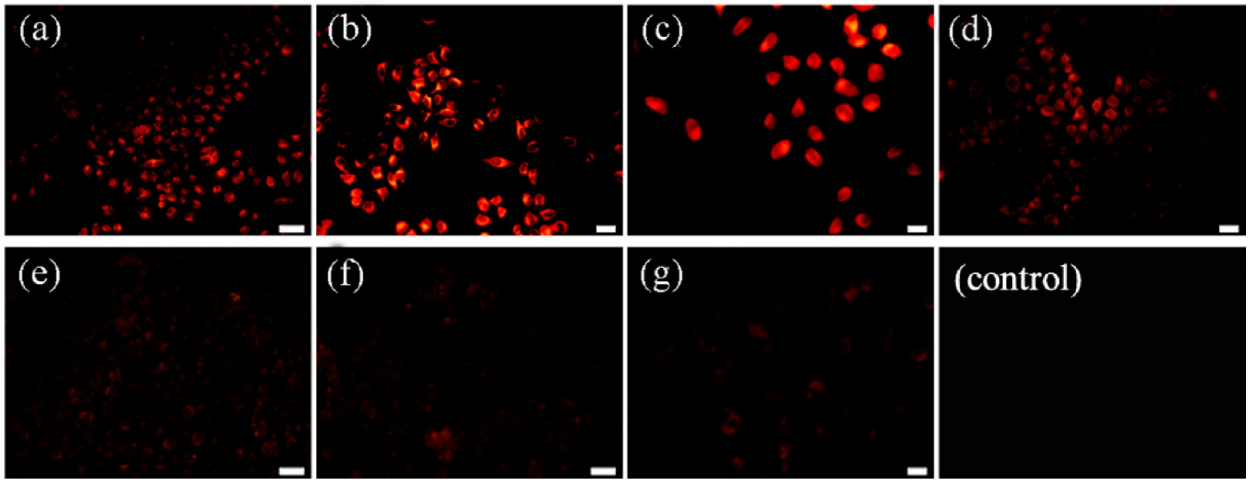


**Figure 8.** Fluorescence images of HeLa cells incubated with 0.05 mg/mL meso-MSPs for (a) 1, (b) 2, (c) 3, (d) 4, (e) 5, (f) 7, and (g) 9 d and then stained with 0.015 mg/mL fluorescence probe (FP-1) for 30 min. The control was the fluorescence images of HeLa cells incubated with 0.05 mg/mL meso-MSPs for 3 d without the staining by probe FP-1. Excitation wavelength was 520 nm; all the scale bars were 20 $\mu$m, and the exposure time was 10 ms.

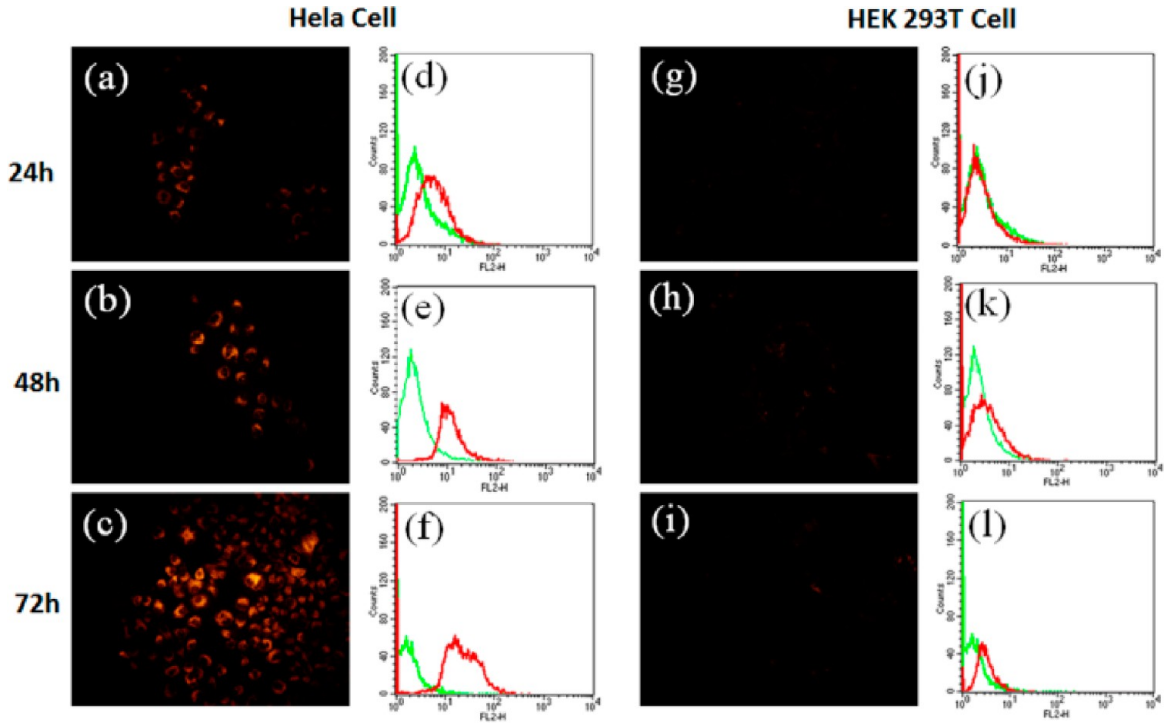


**Figure 9.** Fluorescence microscope images and flow cytometry plots of (a–f) HeLa cells and (g–l) HEK 293T cells incubated with meso-MSPs/probe for 24, 48, and 72 h, respectively. (In the flow cytometry plots, the green line represents the control and the red line represents the cells treated with meso-MSPs/probe.)

fluorescence signals were detected in the pH 5.0 buffer solution as the time increased. As a control experiment, when only the FP-1 was added in the two buffer solutions, no fluorescence could be found; these results demonstrated that the fluorescence was caused by $Fe^{3+}$ but not acidity. Interestingly, the fluorescence intensity possessed a maximum value, i.e., the fluorescence intensity increased at first and then declined with further extension of the treatment time in the pH 5.0 buffer solution. This phenomenon was similar to the trend observed in the results of meso-MSPs/probe incubated with HeLa cells (Figure 6). Meanwhile, inductively coupled plasma (ICP) measurement was employed to monitor the concentration of Fe ions that were released from meso-MSPs into solution (Figure 10b). No detectable Fe ion was found in the pH 7.4 buffer solution, while the concentration of Fe ions progressively increased step by step in the pH 5.0 buffer solution with prolonged incubation time. A possible reason for the trend of fluorescence intensity vs. $Fe^{3+}$ ion concentration is that the fluorescence intensity reaches the maximum at a point where all of the probes have combined with the $Fe^{3+}$ ion. The continued increase of $Fe^{3+}$ ion will quench the fluorescence of the complex and lead to a decrease in fluorescence intensity. The metal ions (such as $Fe^{3+}$ and $Cu^{2+}$) have strong quenching ability via electron transfer, and similar behavior of FP-1 has

**Scheme 1. Conceptual Drawing of the Fluorescent Behaviors of the Meso-MSPs/Probe in HeLa Cells and HEK 293T Cells**

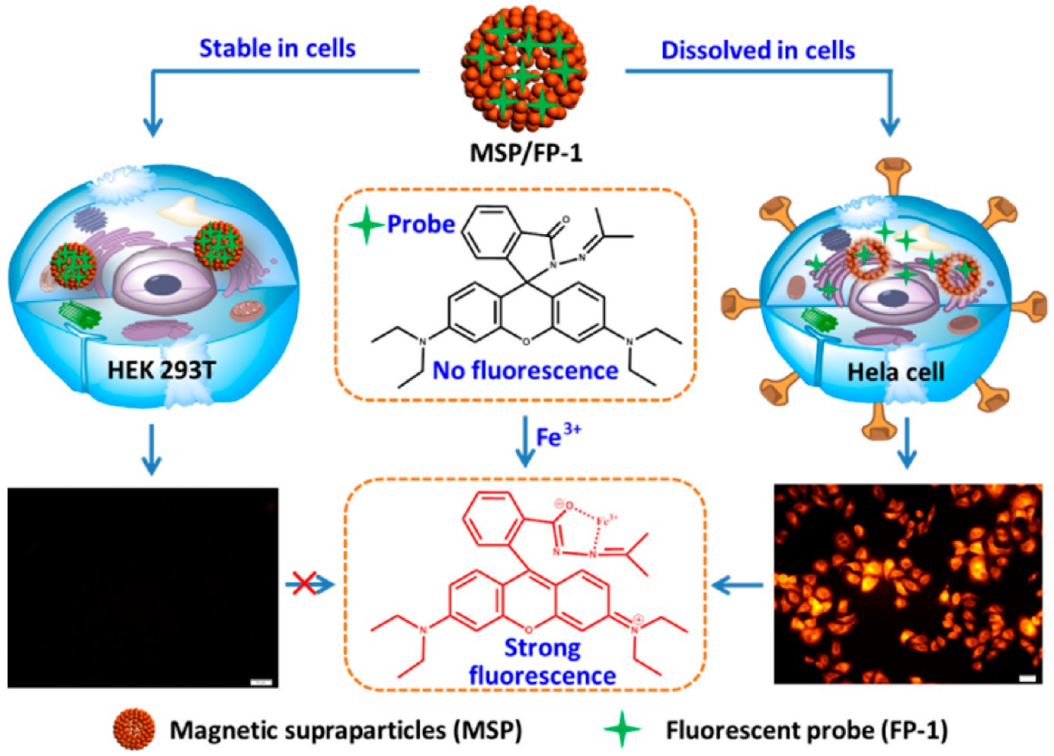


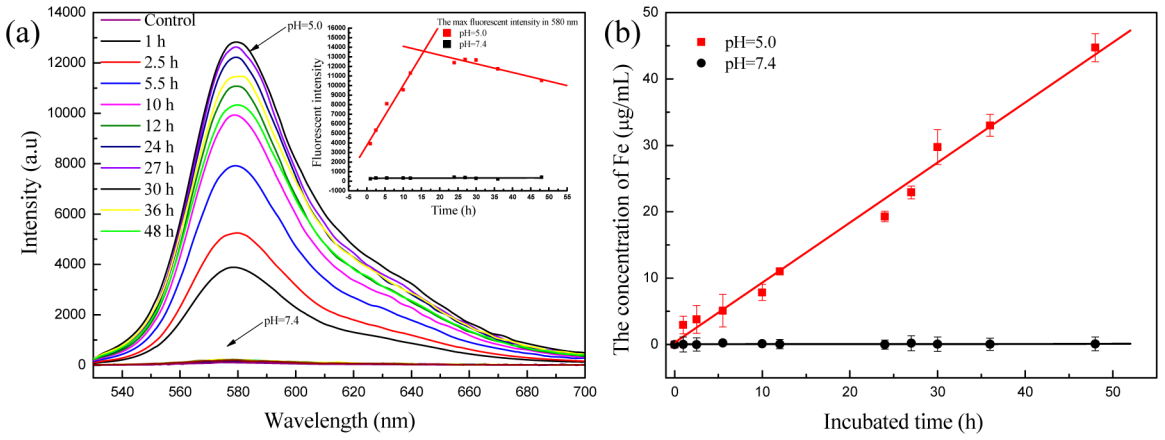


**Figure 10.** (a) Fluorescence spectra and (b) $Fe^{3+}$ ion concentration in the supernatant of meso-MSPs/probe in pH 5.0 and pH 7.4 buffer solutions at various incubation times. (Inset of (a) shows a plot of fluorescence intensity with various incubation times.)

been reported in published papers.[42] Meanwhile, we can reasonably deduce that this similar quenching process might take place in HeLa cells.

In order to check the real status of Fe ions in HeLa cells, we measured the content of elemental iron in HeLa cells by ICP. As shown in Figure 11, Fe ions could be detected after 1 day incubation, implying that the MSPs started to dissolve in the HeLa cells. As the incubation time was prolonged to 4 days, the content of Fe ions in the HeLa cells continued to increase, reflecting more and more MSPs were endocytosed and degraded. Interestingly, from day 4 to day 9, the fluorescence began to weaken, and the corresponding content of Fe ions in the HeLa cells still increased. This result verified that the excess $Fe^{3+}$ ion will quench the fluorescence of the complex FP-1/$Fe^{3+}$, leading to the decrease of fluorescence intensity. However, because of the complicated environment of cells, the simulated cellular environment experiment might not coincide perfectly with the actual situation, so the changes of cellular environment, such as pH, reducibility, metabolic capability or enzymatic activity, would also probably affect the quantum efficiency of probes for long-time incubation (detailed experiments are also underway in our laboratory).

## 4. CONCLUSION

In this paper, composite nanoparticles that consisted of $Fe^{3+}$-sensitive fluorescent probe (FP-1) and $\gamma$-PGA stabilized meso-MSPs were designed and fabricated. The degradation of meso-MSPs in HeLa cells with acidic intracellular environment can be monitored in situ via the change of fluorescence intensity. The fluorescence intensity of HeLa cells went up with the increase of the release amount of $Fe^{3+}$ from meso-MSPs; however, the excess $Fe^{3+}$ ions will quench the fluorescence of the complex

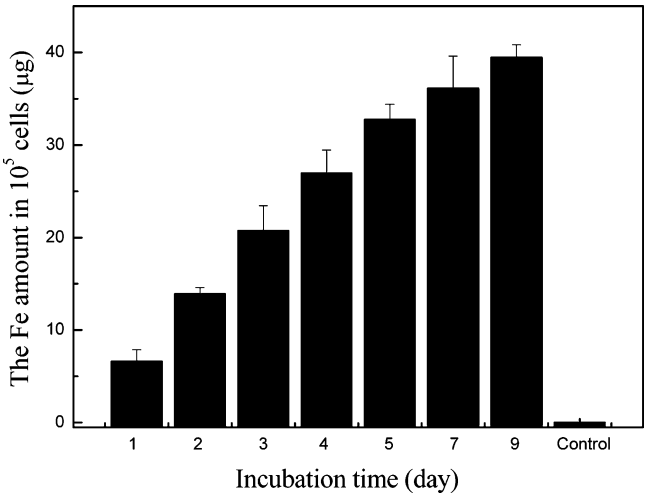


**Figure 11.** The amount of iron (Fe) in HeLa cells treated by meso-MSPs with different incubation times. ("Control" represents the HeLa cells without meso-MSPs treatment.)

FP-1/$Fe^{3+}$, leading to the decrease of fluorescence intensity in HeLa cells. In contrast, HEK 293T cells with relative neutral intracellular environment generated only a very weak fluorescence, because the degradation of meso-MSPs was unlikely to occur. The degradation–luminescence relationship of meso-MSPs/probe facilitates the understanding of degradation behavior of meso-MSPs in cells. Meanwhile, the as-prepared composite nanoparticles pave a new pathway for in situ monitoring the pH conditions of the cells.

## AUTHOR INFORMATION

### Corresponding Author

*E-mail: ccwang@fudan.edu.cn.

### Notes

The authors declare no competing financial interest.

## ACKNOWLEDGMENTS

This work was supported by the National Science and Technology Key Project of China (Grant No. 2012AA020204), the National Science Foundation of China (Grant Nos. 21128001 and 51073040), and the Science and Technology Commission of Shanghai (Grant Nos. 13JC1400500 and 13520720200).

## REFERENCES

(1) Frey, N. A.; Peng, S.; Cheng, K.; Sun, S. H. *Chem. Soc. Rev.* **2009**, *38*, 2532–2542.
(2) Cheng, K.; Peng, S.; Xu, C. J.; Sun, S. H. *J. Am. Chem. Soc.* **2009**, *131*, 10637–10644.
(3) Thomas, C. R.; Ferris, D. P.; Lee, J. H.; Choi, E.; Cho, M. H.; Kim, E. S.; Stoddart, J. F.; Shin, J. S.; Cheon, J.; Zink, J. I. *J. Am. Chem. Soc.* **2010**, *132*, 10623–10625.
(4) Luo, Z.; Cai, K. Y.; Hu, Y.; Li, J. H.; Ding, X. W.; Zhang, B. L.; Xu, D. W.; Yang, W. H.; Liu, P. *Adv. Mater.* **2012**, *24*, 431–435.
(5) Yoon, T. J.; Kim, J. S.; Kim, B. G.; Yu, K. N.; Cho, M. H.; Lee, J. K. *Angew. Chem., Int. Ed.* **2005**, *44*, 1068–1071.
(6) Ruiz-Hernandez, E.; Baeza, A.; Vallet-Regi, M. S. *ACS Nano* **2011**, *5*, 1259–1266.
(7) Deshmukh, M.; Singh, Y.; Gunaseelan, S.; Gao, D.; Stein, S.; Sinko, P. J. *Biomaterials* **2010**, *31*, 6675–6684.
(8) Zeng, Y. F.; Tseng, S. J.; Kempson, I. M.; Peng, S. F.; Wu, W. T.; Liu, J. R. *Biomaterials* **2012**, *33*, 9239–9245.
(9) Pan, Y. J.; Chen, Y. Y.; Wang, D. R.; Wei, C.; Guo, J.; Lu, D. R.; Chu, C. C.; Wang, C. C. *Biomaterials* **2012**, *33*, 6570–6579.
(10) Singh, N. K.; Das. Purkayastha, B.; Roy, J. K.; Banik, R. M.; Yashpal, M.; Singh, G.; Malik, S.; Maiti, P. *ACS Appl. Mater. Interfaces* **2010**, *1*, 69–81.
(11) Kim, J.; Kim, H. S.; Lee, N.; Kim, T.; Kim, H.; Yu, T.; Song, I. C.; Moon, W. K.; Hyeon, T. *Angew. Chem., Int. Ed.* **2008**, *47*, 8438–8441.
(12) Liu, J.; Qiao, S. Z.; Hu, Q. H.; Lu, G. Q. *Small* **2011**, *7*, 425–443.
(13) Ma, W. F.; Zhang, Y.; Li, L. L.; You, L. J.; Zhang, P.; Zhang, Y. T.; Li, J. M.; Yu, M.; Guo, J.; Lu, H. J; Wang, C. C. *ACS Nano* **2012**, *6*, 3179–3188.
(14) Linley, S.; Leshuk, T.; Gu, F. X. *ACS Appl. Mater. Interfaces* **2013**, *5*, 2540–2548.
(15) Liu, T. Y.; Hu, S. H.; Liu, D. M.; Chen, S. Y.; Chen, I. W. *Nano Today* **2009**, *4*, 52–65.
(16) Zhang, Y. T.; Yang, Y. K.; Ma, W. F.; Guo, J.; Lin, Y.; Wang, C. C. *ACS Appl. Mater. Interfaces* **2013**, *5*, 2626–2633.
(17) Zhang, L.; Xue, H.; Cao, Z. Q.; Keefe, A.; Wang, J. N.; Jiang, S. Y. *Biomaterials* **2011**, *32*, 4604–4608.
(18) Lin, C. W.; Tseng, J.; Kempson, I.; Yang, S. C.; Hong, T. M.; Yang, P. C. *Biomaterials* **2013**, *34*, 4387–4393.
(19) Horcajada, P.; Chalati, T.; Serre, C.; Gillet, B.; Sebrie, C.; Baati, T.; et al. *Nat. Mater.* **2010**, *9*, 172–178.
(20) Meng, F. H.; Hennink, W. E.; Zhong, Z. *Biomaterials* **2009**, *30*, 2180–2198.
(21) Oh, J. K.; Tang, C. B.; Gao, H. F.; Tsarevsky, N. V.; Matyjaszewski, K. *J. Am. Chem. Soc.* **2006**, *128*, 5578–5584.
(22) Luo, B.; Xu, S.; Luo, A.; Wang, W. R.; Wang, S. L.; Guo, J.; Wang, C. C. *ACS Nano* **2011**, *5*, 1428–1435.
(23) Li, D.; Tang, J.; Wei, C.; Guo, J.; Wang, S. L.; Chaudhary, D.; Wang, C. C. *Small* **2012**, *8*, 2690–2698.
(24) Ge, J. P.; Hu, Y. X.; Biasini, M.; Beyermann, W. P.; Yin, Y. D. *Angew. Chem., Int. Ed.* **2007**, *46*, 4342–4345.
(25) Liu, J.; Sun, Z. K.; Deng, Y. H.; Zou, Y.; Li, C. Y.; Guo, X. H.; et al. *Angew. Chem., Int. Ed.* **2009**, *48*, 5875–5879.
(26) Zipfel, W. R.; Williams, R. M.; Webb, W. W. *Nat. Biotechnol.* **2003**, *21*, 1368–1376.
(27) Kobayashi, H.; Ogawa, M.; Alford, R.; Choyke, P. L.; Urano, Y. *Chem. Rev.* **2010**, *110*, 2620–2640.
(28) Yang, Y. M.; Zhao, Q.; Feng, W.; Li, F. Y. *Chem. Rev.* **2013**, *113*, 192–270.
(29) Cho, D. G.; Sessler, J. L. *Chem. Soc. Rev.* **2009**, *38*, 1647–1662.
(30) Xu, Z. C.; Chen, X. Q.; Kim, H. N.; Yoon, J. Y. *Chem. Soc. Rev.* **2010**, *39*, 127–137.
(31) Chen, X. Q.; Tian, X. Z.; Shin, I.; Yoon, J. Y. *Chem. Soc. Rev.* **2011**, *40*, 4783–4804.
(32) Yu, H. B.; Xiao, Y.; Guo, H. Y.; Qian, X. H. *Chem.—Eur. J.* **2011**, *17*, 3179–3191.
(33) Dujols, V.; Ford, F.; Czarnik, A. W. *J. Am. Chem. Soc.* **1997**, *119*, 7386–7387.
(34) Moon, K. S.; Yang, Y. K.; Ji, S.; Tae, J. *Tetrahedron Lett.* **2010**, *51*, 3290–3293.
(35) Zhou, Z. G.; Yu, M. X.; Yang, H.; Huang, K. W.; Li, F. Y.; Yi, T.; Huang, C. H. *Chem. Commun.* **2008**, *44*, 3387–3389.
(36) Lee, H. Y.; Bae, D. R.; Park, J. C.; Song, H.; Han, W. S.; Jung, J. H. *Angew. Chem., Int. Ed.* **2009**, *48*, 1239–1243.
(37) Hirayama, T.; Okuda, K.; Nagasawa, H. *Chem. Sci.* **2012**, *3*, 2257–2261.
(38) Du, P. W.; Lippard, S. J. *Inorg. Chem.* **2010**, *49*, 10753–10755.
(39) Zhang, M.; Gao, Y. H.; Li, M. Y.; Yu, M. X.; Li, F. Y.; Li, L.; Zhu, M. W.; Zhang, J. P.; Yi, T.; Huang, C. H. *Tetrahedron Lett.* **2007**, *48*, 3709–3712.
(40) Lee, M. H.; Van Giap, T.; Kim, S. H.; Lee, Y. H.; Kang, C.; Kim, J. S. *Chem. Commun.* **2010**, *46*, 1407–1409.
(41) Jackson, R. K.; Shi, Y.; Yao, X. D. *Dalton Trans.* **2010**, *39*, 4155–4161.

(42) Hu, Z. Q.; Feng, Y. C.; Huang, H. Q.; Ding, L.; Wang, X. M.; Lin, C. S.; Li, M.; Ma, C. P. *Sens. Actuators B* **2011**, *156*, 428−432.
(43) Jiao, Y. F.; Guo, J.; Shen, S.; Chang, B. S.; Zhang, Y. H.; Jiang, X. G.; Yang, W. L. *J. Mater. Chem.* **2012**, *22*, 17636−17643.
(44) Hong, R.; Han, G.; Fernandez, J. M.; Kim, B. J.; Forbes, N. S.; Rotello, V. M. *J. Am. Chem. Soc.* **2006**, *128*, 1078−1079.
(45) Simon, S. M. *Drug Discovery Today* **1999**, *4*, 32−38.